DE82014720

EFFECTS OF GAPS IN ADHESIVES THAT BOND ELASTICALLY DEFORMED PANELS TO PARABOLIC, CYLINDRICAL SUBSTRUCTURES

SANDIA NATIONAL LABS.
ALBUQUERQUE, NM

MAR 1982

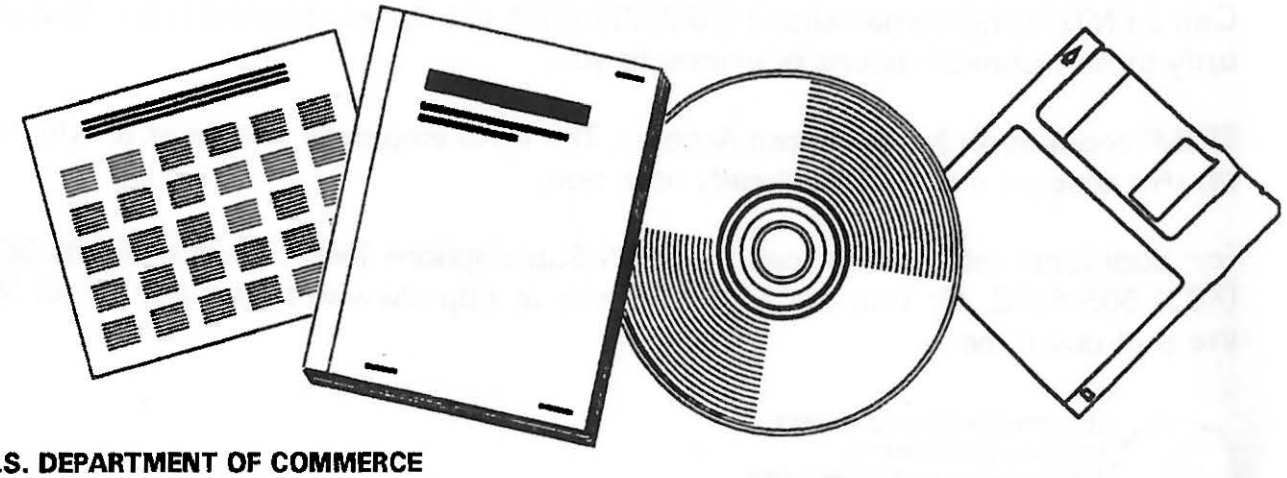

U.S. DEPARTMENT OF COMMERCE
National Technical Information Service

Tailored to Your Needs!

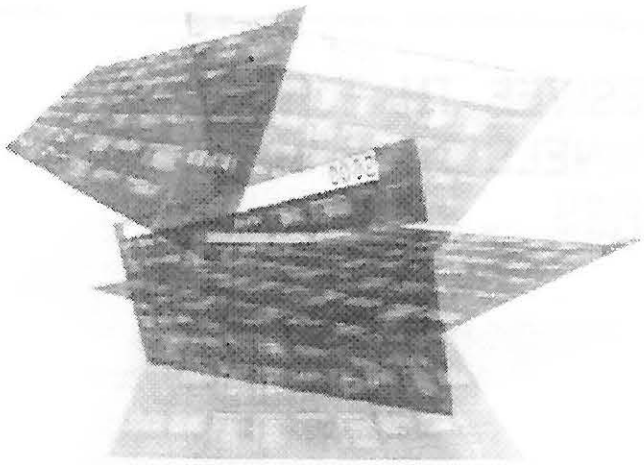

Selected Research In Microfiche

SRIM® is a tailored information service that delivers complete microfiche copies of government publications based on your needs, automatically, within a few weeks of announcement by NTIS.

SRIM® Saves You Time, Money, and Space!

Automatically, every two weeks, your SRIM® profile is run against all *new* publications received by NTIS and the publications microfiched for your order. Instead of paying approximately $15-30 for each publication, you pay only $2.50 for the microfiche version. Corporate and special libraries love the space-saving convenience of microfiche.

NTIS offers two options for SRIM® selection criteria:

Standard SRIM®–Choose from among 350 pre-chosen subject topics.

Custom SRIM®–For a one-time additional fee, an NTIS analyst can help you develop a keyword strategy to design your Custom SRIM® requirements. Custom SRIM® allows your SRIM® selection to be based upon *specific subject keywords*, not just broad subject topics. Call an NTIS subject specialist at (703) 605-6655 to help you create a profile that will retrieve only those technical reports of interest to you.

SRIM® requires an NTIS Deposit Account. The NTIS employee you speak to will help you set up this account if you don't already have one.

For additional information, call the NTIS Subscriptions Department at 1-800-363-2068 or (703) 605-6060. Or visit the NTIS Web site at *http://www.ntis.gov* and select SRIM® from the pull-down menu.

U.S. DEPARTMENT OF COMMERCE
Technology Administration
National Technical Information Service
Springfield, VA 22161 (703) 605-6000
http://www.ntis.gov

SAND82-0291

THE EFFECTS OF GAPS IN ADHESIVES THAT BOND ELASTICALLY DEFORMED PANELS TO PARABOLIC, CYLINDRICAL SUBSTRUCTURES*

R. K. Wilson
R. C. Reuter, Jr.
Sandia National Laboratories
Albuquerque, NM 87185

ABSTRACT

In previous studies of the mechanical behavior of line focusing solar collectors, the reflective surface panel was modeled as a thin, initially flat, elastic plate that underwent large displacements to attain the shape of a prescribed parabolic cylinder. Attention was focused upon the stresses that developed in an adhesive layer which bonded the deformed panel to a rigid, parabolic substructure. Among the myriad possible collector designs, some possess longitudinally oriented, hollow ribs or corrugations in the substructure which interrupt the transverse continuity of the bond line between the deformed panel and the substructure. Thus, finite gaps in the adhesive are present which create regions where the panel surface becomes intermittently supported. The presence of these gaps perturbs the otherwise smooth distribution of adhesive contact stresses and it is the analytical modeling of this behavior that is the subject of the present report. In particular, attention is devoted to gaps which overlap with the edge effect zone - a region near the rim or vertex of the deformed panel where, in the absence of uniform edge loads necessary to maintain a true parabolic shape, high stresses and associated deformations occur. Significant influences of the gap size and position in the edge effect zone are demonstrated and discussed.

---

* This work was performed at Sandia National Laboratories and was supported by the U.S. Department of Energy under contract number DE-AC04-76DP00789.

TABLE OF CONTENTS

LIST OF FIGURES

LIST OF FIGURES (Cont.)

NOMENCLATURE

A_i, B_i, C_i, D_i	integration constants appearing in expressions for w_i and σ_i
D	flexural rigidity of reflective panel
E	Young's modulus of reflective panel
f	focal length of parabola
h	thickness of adhesive
k_i	stiffness of reflective surface for section i
M_R	bending moment applied to rim to maintain true parabolic shape
M_V	bending moment applied to vertex to maintain true parabolic shape
P_C	contact pressure applied over back surface of reflective panel to maintain true parabolic shape
Q_R	shear force applied at rim to maintain true parabolic shape
$w_i(x)$	displacement at x of reflective surface due to edge effects and gap
$w_R(x)$	displacement at x of reflective surface due to edge effect at rim
$w_V(x)$	displacement at x of reflective surface due to edge effect at vertex
w'_{rms}	rms value of slope error
x, y	rectangular coordinates
z_1, z_2	coordinates of the ends of the gap
β_i	panel-adhesive-substructure stiffness parameter
δ_2	second cross-over distance
ζ	coordinate measured from rim
$\sigma_i(x)$	normal contact stress at x due to edge effects and gap
$\sigma_R(x)$	normal contact stress at x due to edge effect at rim
$\sigma_V(x)$	normal contact stress at x due to edge effect at vertex

INTRODUCTION

Figure 1 shows a completed, parabolic, line focusing solar collector utilizing a stamped, sheet metal substructure and an elastically deformed reflective surface. Two, initially flat, reflective panels undergo large displacements each forming one half of a parabolic, cylindrical surface. Abutting the vertices of the two half-parabolic surfaces and bonding them to the concave side of a rigid, prefabricated, parabolic substructure produces a collector whose reflective surface is defined by

$$y = \frac{x^2}{4f} \quad . \tag{1}$$

Two analytical studies of this general collector design concept, with experimental verification, have already appeared [1,2]. The reflective surface, bonded to the substructure with a continuous adhesive layer, was treated as a single, rim to rim panel in [1], and as a dual panel with a seam at the vertex (as described above) in [2]. Distributed surface pressures and uniform edge loads (called forming loads) necessary to mechanically form the reflective surface to the desired parabolic shape were calculated along with the stress distributions developed in the bonding adhesive after the forming loads were removed. Removal of the surface pressure distribution resulted in negligible stresses, Fig. 3, in the adhesive (for the specific construction of interest). However, removal of the uniform edge loads at the rim and vertex (in [2]) resulted in much larger stresses, Fig. 4, and a corresponding loss of the parabolic shape, characterized by a rotation of surface normals (called slope errors), Fig. 5. These variations were localized near the rim and vertex, and were called edge effects.* In both of these studies the rigid,

---

* A summary of the forming loads, resulting stresses and slope errors is given in Appendix A.

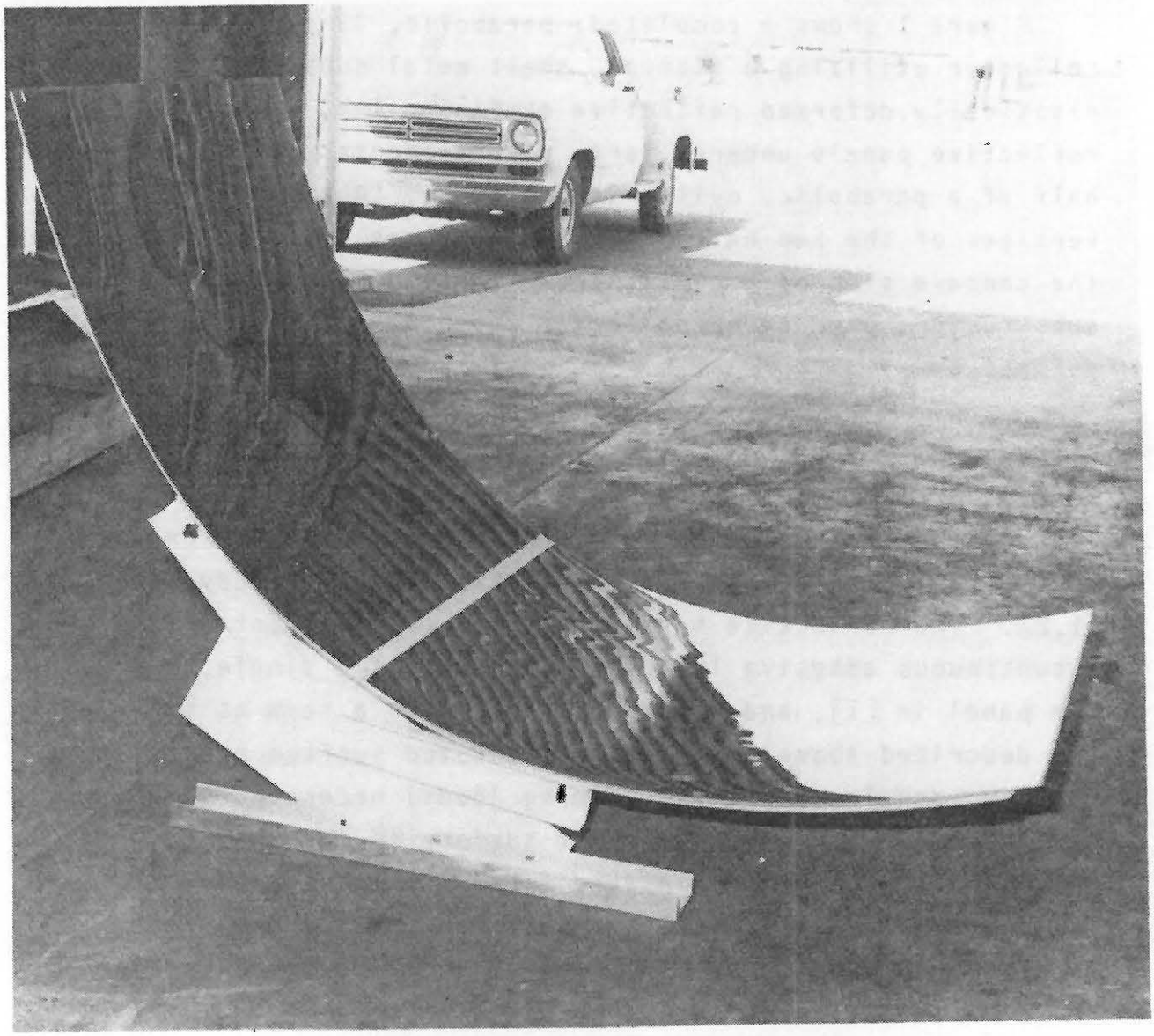

Figure 1. Assembled, Parabolic Line Focusing Solar Collector

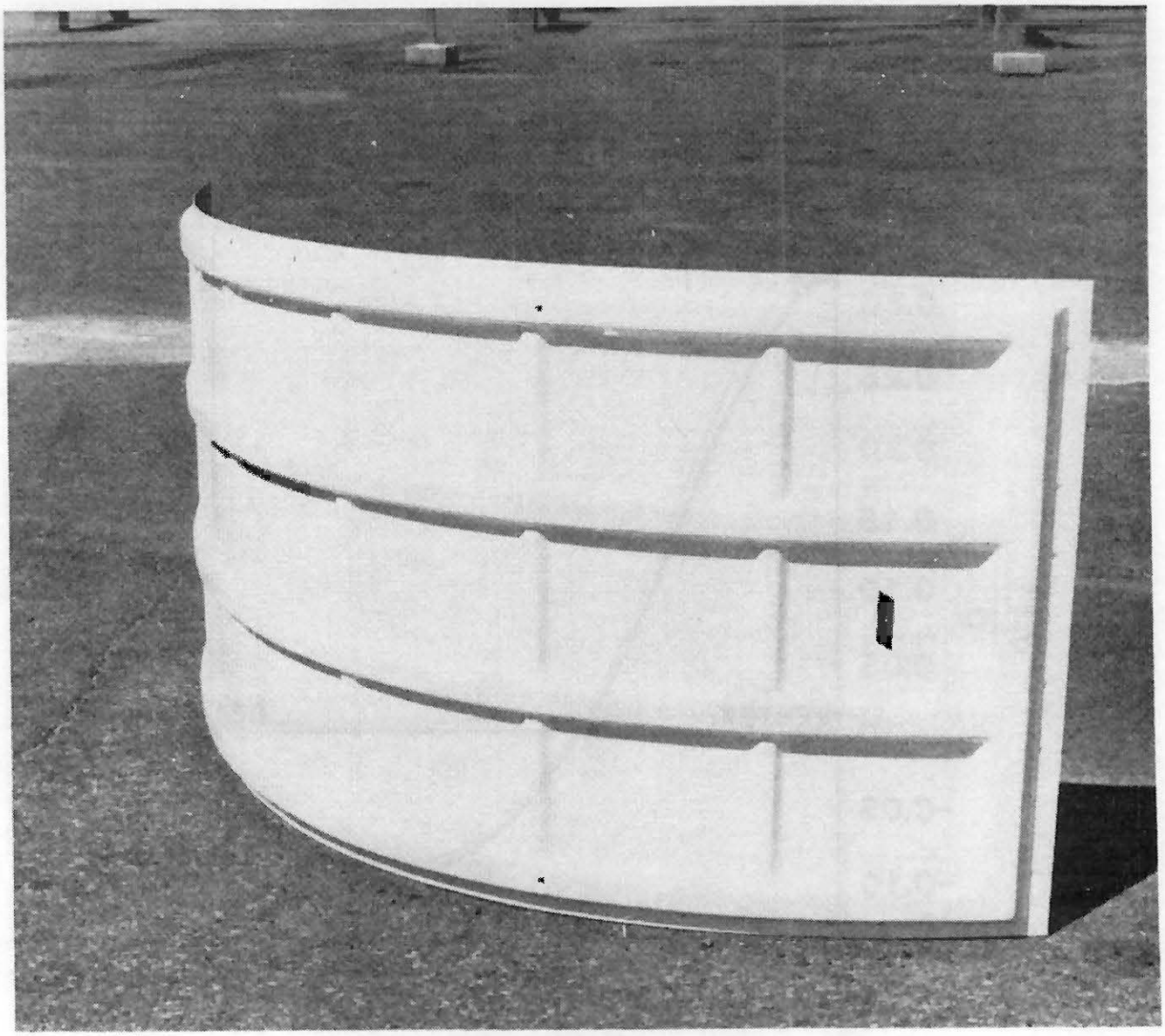

Figure 2. View of Stamped, Sheet Metal Substructure Showing Stiffening Rims.

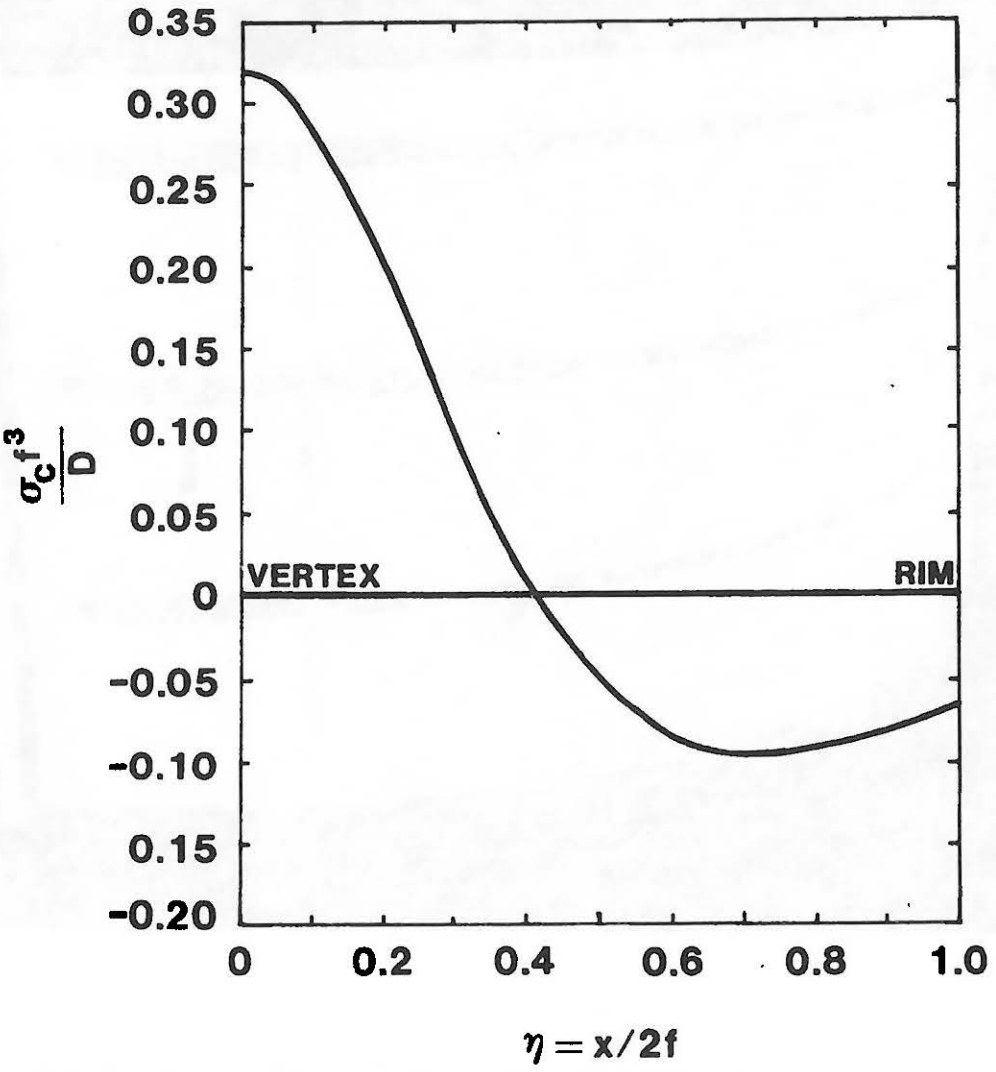

Figure 3. Dimensionless Contact Stresses in Adhesive Applied to Backside of Reflective Surface after Forming.

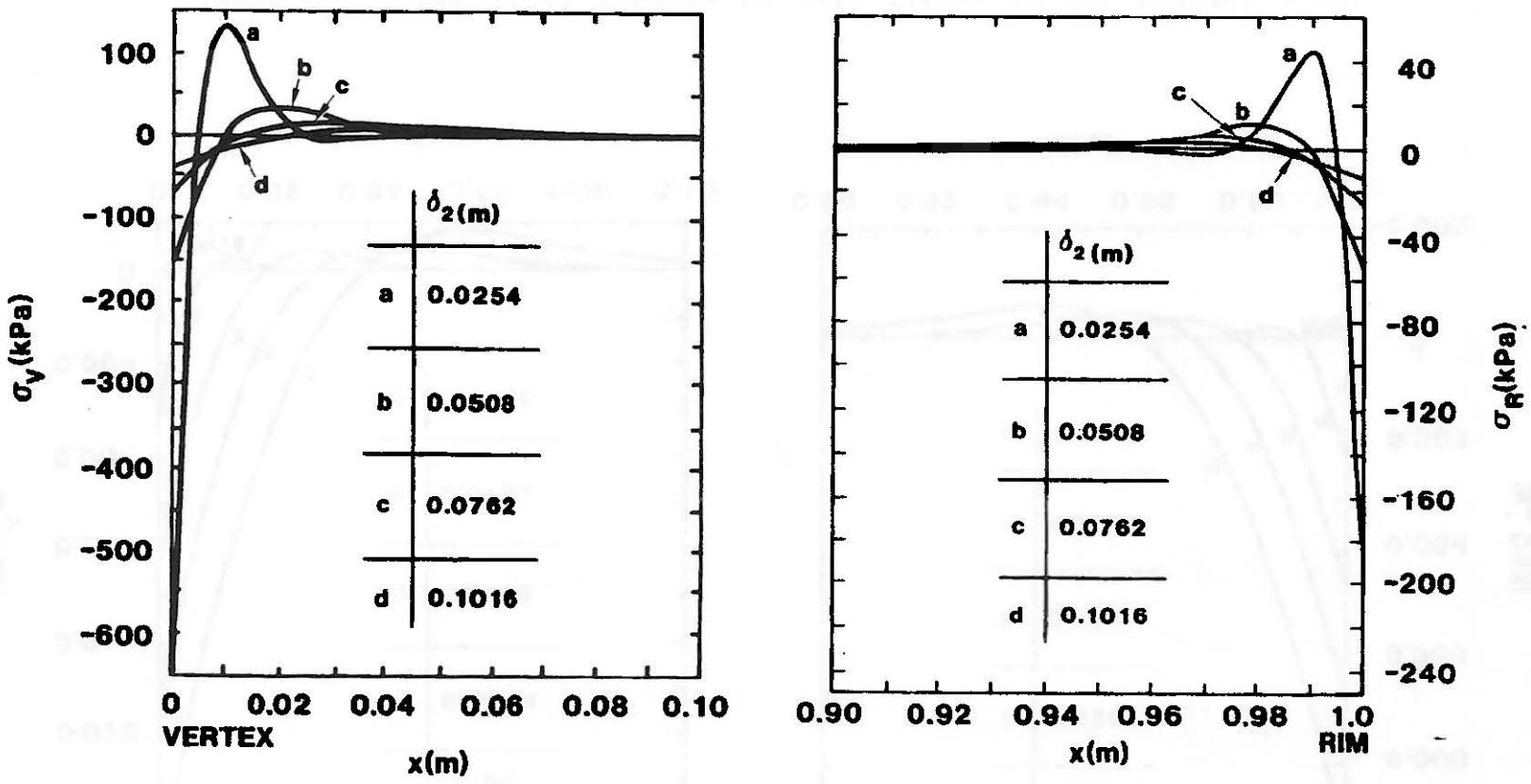

Figure 4. Contact Stresses in Adhesive Applied to Backside of Deformed Reflective Surface Arising from Edge Effect.

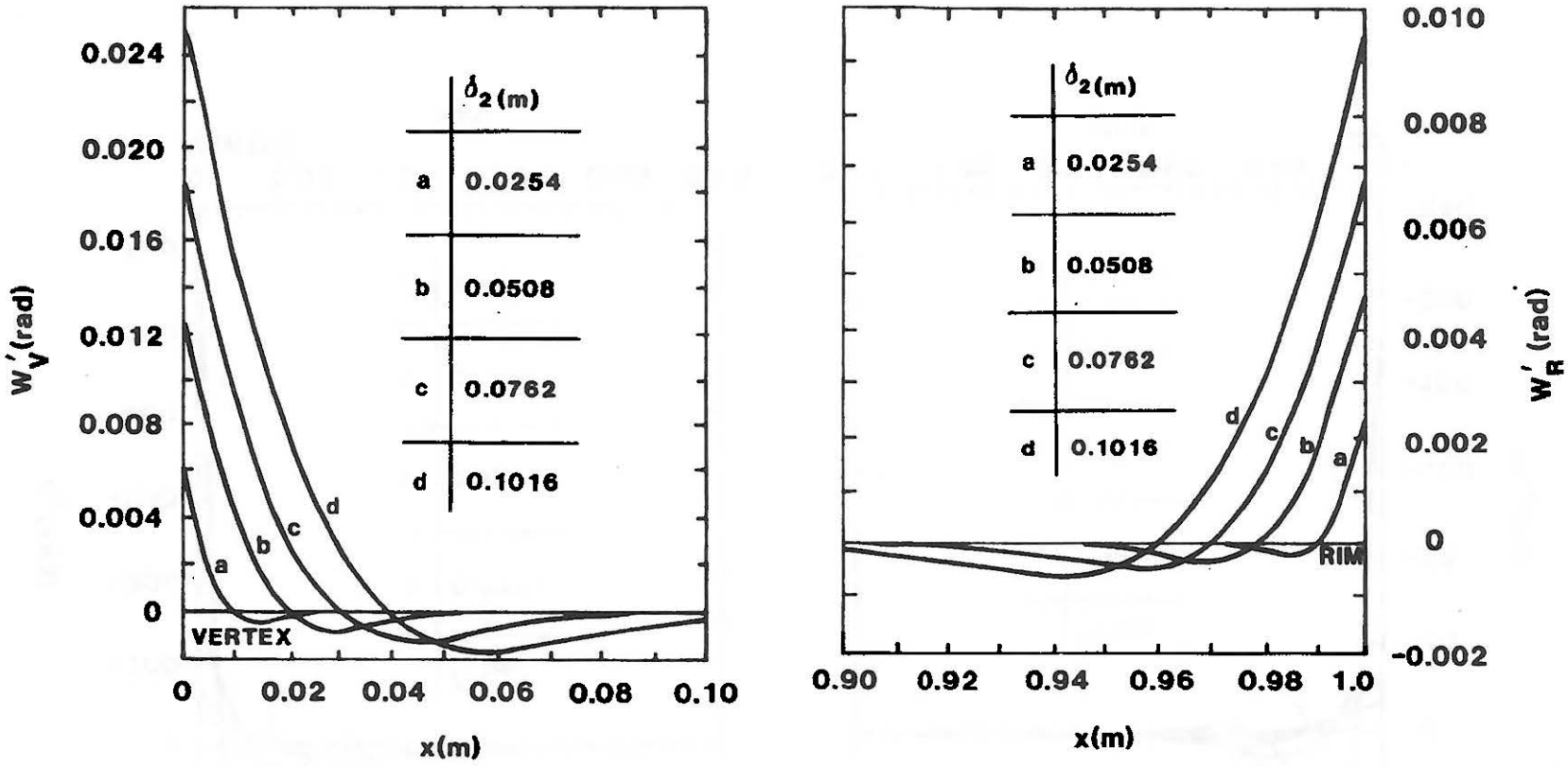

Figure 5. Rotation of Surface Normals (Slope Error) Arising from Edge Effect.

parabolic substructure consisted of a smooth, continuous sheet metal facing backed by a stamped panel into which hollow, stiffening ribs were formed. The analyses [1,2] are, of course, valid for any construction which possesses a continuous backing for the reflective surface.

In another design [3], the sheet metal facing is eliminated and the deformed, reflective panels are bonded directly to the stamped, parabolic substructure. The presence of longitudinal, hollow ribs bonded directly to the reflective panel creates longitudinal gaps in the adhesive layer which interrupt the transverse continuity of support. The effect of these gaps can be seen in Fig. 6 where slope errors increase when measured over the gaps. The presence of the adhesive gaps affects contact stresses and slope errors to a greater extent when they occur in high stress regions, namely, the edge effect zones (near rim and vertex). In this report the effects of the size and location of adhesive gaps upon contact stresses and slope errors are investigated. Emphasis is placed on numerical results and discussion of cases where gaps occur in or near the edge effect zone.

ANALYSIS

In Fig. 7 a cross section of the collector near the rim is shown both as it actually appears, Fig. 7a, indicating the reflective panel, adhesive layer and rib stiffened substructure, and as it is modeled by a flat plate on an elastic foundation,* Fig. 7b, which has been interrupted to account for the gap in the adhesive. The elastic foundation in Fig. 7b represents both the adhesive and the supporting

$$D \frac{d^4 w_i}{d\zeta_i^4} + k_i w_i = 0; \quad i = 1,2,3 \qquad (2)$$

* The arguments for modeling the structure near the rim by a flat plate are given in [1] and arise from the particular geometry (focal lengths) of the parabolas of interest.

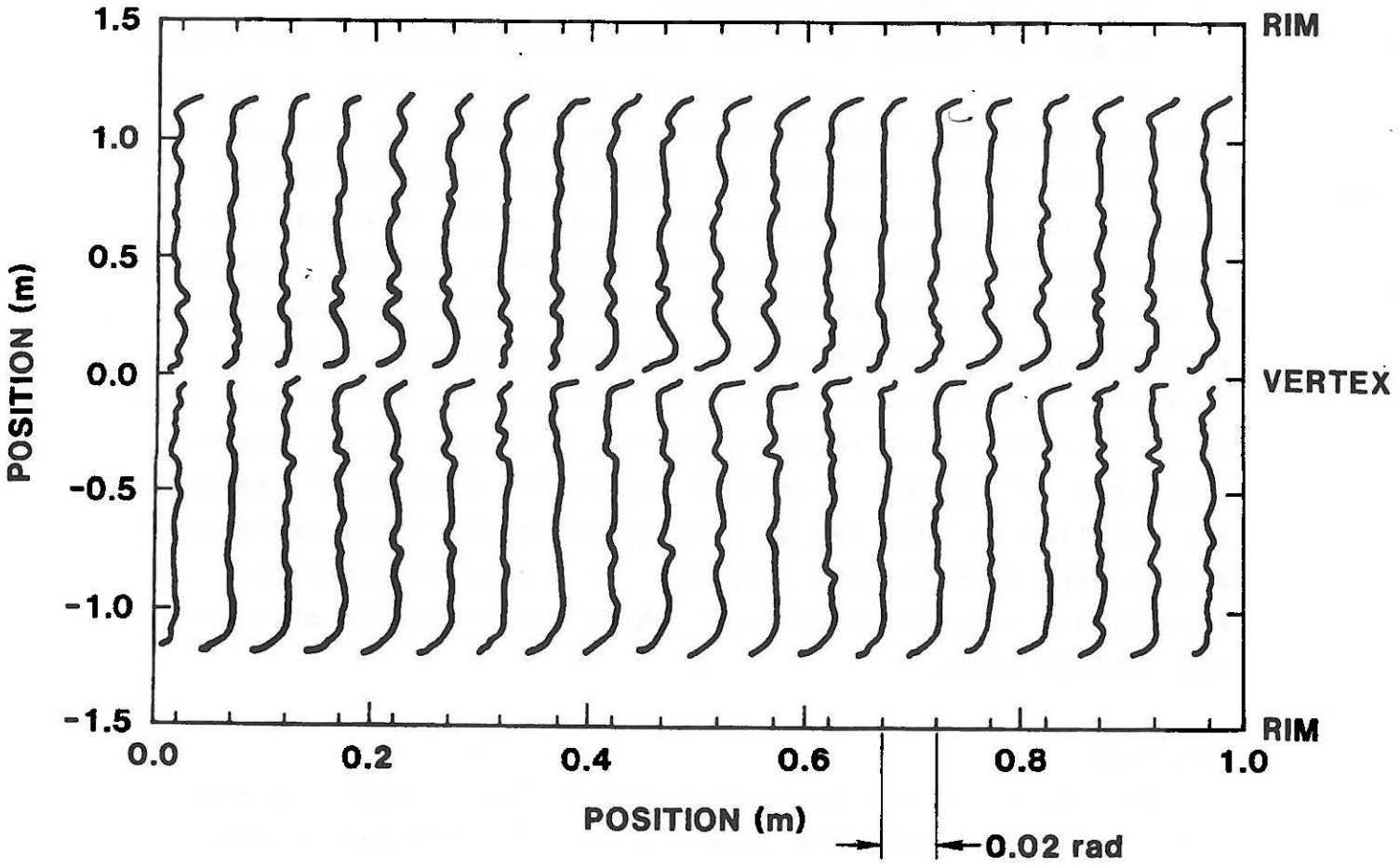

Figure 6. Typical Results from Laser Ray Tracing Showing Slope Errors at Rim and Vertex.

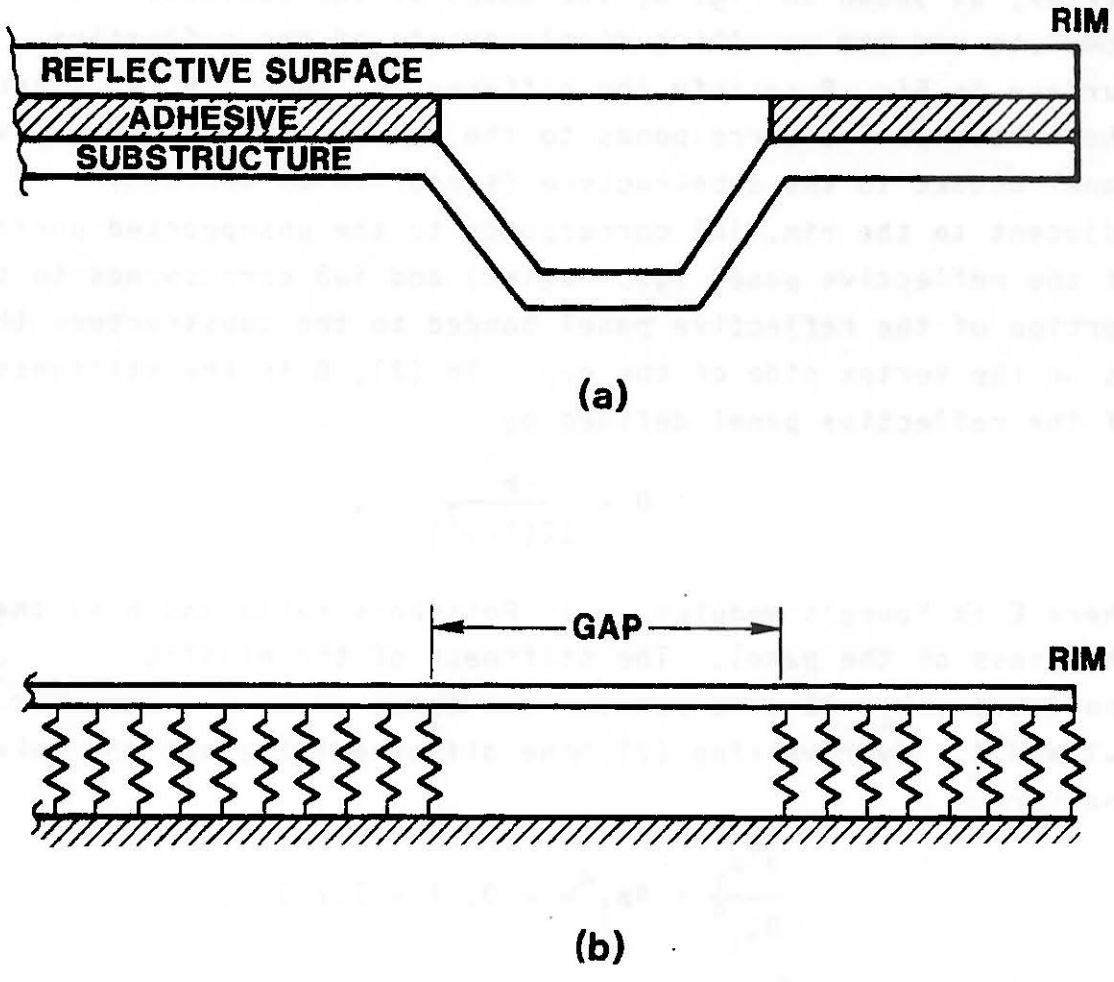

Figure 7. Region of Collector near Rim Showing Gap, Adhesive and Substructure (a) as the Gap Actually Occurs and (b) as It is Modeled by a Flat Plate on an Elastic Foundation, Interrupted to Account for the Gap.

substructure. By applying the edge loads to the rim and vertex, as shown in Fig. 8, the model of the collector is complete and the resulting displacements of the reflective surface in Fig. 8 satisfy the differential equation [4] where the subscript i=1 corresponds to the portion of the reflective panel bonded to the substructure (supported by springs) adjacent to the rim, i=2 corresponds to the unsupported portion of the reflective panel (gap region) and i=3 corresponds to the portion of the reflective panel bonded to the substructure that is on the vertex side of the gap. In (2), D is the stiffness of the reflective panel defined by

$$D = \frac{Eh^3}{12(1-\nu^2)} \quad ,$$

where E is Young's modulus, ν is Poisson's ratio and h is the thickness of the panel. The stiffness of the elastic foundation, k_i, is zero for i=2 and taken to be the same for i=1 and 3. By rewriting (2), the differential equations take the form

$$\frac{d^4 w_i}{D\zeta_i^4} + 4\beta_i^4 w_i = 0; \; i = 1,2,3 \quad , \tag{3}$$

where

$$\beta_i = \begin{cases} \sqrt[4]{\frac{k_i}{4D}} \; ; \; i = 1, 3 \quad , \\ 0 \; ; \; i = 2 \quad . \end{cases} \tag{4}$$

Equation (3) has the well known solution [3]

$$w_i(\zeta) = \begin{cases} e^{-\beta_i\zeta}[A_i\cos\beta_i\zeta + B_i\sin\beta_i\zeta] + e^{\beta_i\zeta}[C_i\cos\beta_i\zeta + D_i\sin\beta_i\zeta]; i=1,3, \\ A_i + B_i\zeta + C_i\zeta^2 + D_i\zeta^3 \; ; \; i=2, \end{cases} \tag{5}$$

where A_i, B_i, C_i and D_i are constants of integration. These twelve constants are determined by satisfying the boundary conditions at the vertex and rim given by

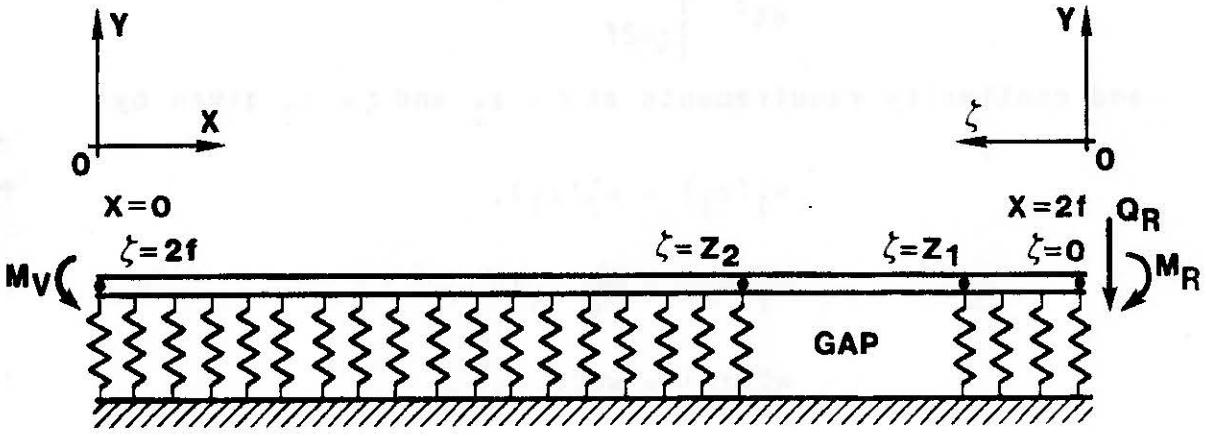

Figure 8. Diagram of Elastic Foundation Model Explicating the Coordinate Systems, Gap Location and Edge Loads

$$\left.\frac{d^2 w_1}{d\zeta^2}\right|_{\zeta=0} = -\frac{M_R}{D}\,, \tag{6}$$

$$\left.\frac{d^3 w_1}{d\zeta^3}\right|_{\zeta=0} = -\frac{Q_R}{D}\,, \tag{7}$$

$$\left.\frac{d^2 w_3}{d\zeta^2}\right|_{\zeta=2f} = -\frac{M_V}{D}\,, \tag{8}$$

$$\left.\frac{d^3 w_3}{d\zeta^3}\right|_{\zeta=2f} = 0\,, \tag{9}$$

and continuity requirements at $\zeta = z_1$ and $\zeta = z_2$ given by

$$w_1(z_1) = w_2(z_1), \tag{10}$$

$$w_1'(z_1) = w_2'(z_1), \tag{11}$$

$$w_1''(z_1) = w_2''(z_1), \tag{12}$$

$$w_1'''(z_1) = w_2'''(z_1), \tag{13}$$

$$w_2(z_2) = w_3(z_2), \tag{14}$$

$$w_2'(z_2) = w_3'(z_2), \tag{15}$$

$$w_2''(z_2) = w_3''(z_2), \tag{16}$$

$$w_2'''(z_2) = w_3'''(z_2). \tag{17}$$

Substituting (5) into (6)-(17) results in 12 linear algebraic equations in the twelve unknowns A_i, B_i, C_i, D_i; i=1,2,3. Table 1 shows values of these constants* for various values of

* These algebraic equations were obtained numerically using the Sandia computer library routine SAXBI (see [5]).

gap size and location, and for three values of δ_2, corresponding to a change in size of the edge effect region. Substituting (5) into the relationships

$$\sigma_i(x) = -k_i w_i(x);\ i=1,3,$$

$$w_i'(x) = \frac{dw_i(x)}{dx};\ i=1,2,3,$$

for the adhesive stress and slope error, respectively, yields

$$\sigma_i(x) = -k_i\Big\{e^{-\beta_i(2f-x)}\,[A_i\cos\beta_i(2f-x) + B_i\sin\beta_i(2f-x)] + e^{-\beta_i(2f-x)}[C_i\cos\beta_i(2f-x) + D_i\sin\beta_i(2f-x)]\Big\}, \tag{18}$$

$$w_i'(x) = \begin{cases} \beta_i\Big\{e^{-\beta_i(2f-x)}[(A_i-B_i)\cos\beta_i(2f-x)+(A_i+B_i)\sin\beta_i(2f-x)] \\ \quad -e^{-\beta_i(2f-x)}[(C_i-D_i)\cos\beta_i(2f-x)+(C_i+D_i)\sin\beta_i(2f-x)]\Big\}; \\ \qquad\qquad\qquad\qquad\qquad\qquad\qquad\qquad\qquad\qquad i=1,3 \\ (B_i + 4C_i f + 12D_i f^2) + (2C_i - 12D_i f)x - 3D_i x^2;\ i=2, \end{cases} \tag{19}$$

where the coordinate $x = (2f - \zeta)$ is measured from the vertex (Fig. 8). The stresses and slope errors defined by (18) and (19) have been evaluated for the values of the constants in Tables 1 and plotted in Figs. 9-22. In each of these figures, stresses or slope errors corresponding to the continuous, gapless model are also plotted, for comparison.

RESULTS

In Figs. 9-20 stresses and slope errors are shown for the values of gap size, location and β given in Table 1. The twelve figures are arranged in three groups of four, each group corresponding to a different value of β. Each group contains two plots of stresses and two plots of slope errors, one plot corresponding to a change in location of the gap and the other to a change in size of the gap.

TABLE 1.a

INTEGRATION CONSTANTS FOR $\beta = 0.196$

A_i cm	87.732	86.462	83.992	81.382	76.300	71.222	89.000	91.542
B_i cm	98.730	97.460	94.920	92.380	87.300	82.220	97.460	97.460
A_1	-0.2230	-0.1748	-0.1414	-0.1331	-0.1339	-0.1363	-0.1714	-0.1649
B_1	0.1378	0.1256	0.1194	0.1177	0.1194	0.1197	0.1252	0.1243
C_1	-4.815×10^{-2}	-2.470×10^{-2}	-5.488×10^{-2}	1.583×10^{-3}	4.142×10^{-3}	2.276×10^{-3}	-2.184×10^{-2}	-1.711×10^{-2}
D_1	2.094×10^{-2}	8.590×10^{-3}	1.474×10^{-3}	8.579×10^{-4}	2.525×10^{-3}	2.789×10^{-3}	8.325×10^{-3}	7.419×10^{-3}
A_2	-0.2711	-0.1996	-0.1472	-0.1323	-0.1292	-0.1210	-0.1933	-0.1820
B_2	6.541×10^{-2}	5.568×10^{-2}	5.077×10^{-2}	5.080×10^{-2}	5.126×10^{-2}	4.558×10^{-2}	5.565×10^{-2}	5.492×10^{-2}
C_2	-4.582×10^{-3}	-4.733×10^{-3}	-5.015×10^{-3}	-5.183×10^{-3}	-4.982×10^{-3}	-4.085×10^{-3}	-4.724×10^{-3}	-4.708×10^{-3}
D_2	8.519×10^{-5}	1.301×10^{-4}	1.618×10^{-4}	1.673×10^{-4}	1.475×10^{-4}	1.095×10^{-4}	1.24×10^{-4}	1.133×10^{-4}
A_3	-0.2600	-0.1918	-0.1471	-0.1447	-0.1885	-0.2491	-0.1888	-0.1801
B_3	2.102×10^{-2}	5.754×10^{-2}	0.1040	0.1390	0.1842	0.1834	7.046×10^{-2}	8.643×10^{-2}
C_3	1.286×10^{-4}	1.257×10^{-4}	1.257×10^{-4}	1.257×10^{-4}	1.257×10^{-4}	1.256×10^{-4}	1.257×10^{-4}	1.257×10^{-4}
D_3	-1.659×10^{-4}	-1.659×10^{-4}	-1.660×10^{-4}	-1.659×10^{-4}	-1.659×10^{-4}	-1.659×10^{-4}	-1.659×10^{-4}	-1.659×10^{-4}

TABLE 1.b

INTEGRATION CONSTANTS FOR $\beta = 0.392$

A_i cm	87.732	86.462	83.992	81.382	76.300	71.222	89.000	91.542
B_i cm	98.730	97.460	94.920	92.380	87.300	82.220	97.460	97.460
A_1	-3.989×10^{-2}	-3.262×10^{-2}	-3.274×10^{-2}	-3.393×10^{-2}	-3.255×10^{-2}	-3.140×10^{-2}	-3.263×10^{-2}	-3.296×10^{-2}
B_1	3.143×10^{-2}	3.057×10^{-2}	3.127×10^{-2}	3.124×10^{-2}	2.984×10^{-2}	2.928×10^{-2}	2.996×10^{-2}	2.963×10^{-2}
C_1	-4.337×10^{-3}	1.312×10^{-3}	2.589×10^{-3}	1.346×10^{-3}	-7.733×10^{-5}	-5.959×10^{-5}	8.068×10^{-5}	-9.231×10^{-4}
D_1	2.211×10^{-3}	1.349×10^{-3}	2.048×10^{-3}	2.023×10^{-3}	6.226×10^{-4}	5.582×10^{-5}	7.430×10^{-4}	4.059×10^{-4}
A_2	-4.433×10^{-2}	-3.136×10^{-2}	-3.006×10^{-2}	-3.017×10^{-2}	-1.207×10^{-2}	1.528×10^{-2}	-3.261×10^{-2}	-3.396×10^{-2}
B_2	2.723×10^{-2}	2.804×10^{-2}	2.693×10^{-2}	2.437×10^{-2}	1.015×10^{-2}	-2.184×10^{-3}	2.512×10^{-2}	2.462×10^{-2}
C_2	-4.702×10^{-3}	-4.876×10^{-3}	-4.766×10^{-3}	-3.913×10^{-3}	-1.433×10^{-3}	7.667×10^{-5}	-4.920×10^{-3}	-4.960×10^{-3}
D_2	2.580×10^{-4}	2.727×10^{-4}	2.44×10^{-4}	1.808×10^{-4}	5.641×10^{-5}	1.001×10^{-7}	2.998×10^{-4}	3.249×10^{-4}
A_3	-5.333×10^{-2}	-6.449×10^{-2}	-0.1129	-0.1587	-0.1450	-5.436×10^{-2}	-4.183×10^{-2}	-3.483×10^{-2}
B_3	2.831×10^{-2}	5.832×10^{-2}	7.461×10^{-2}	5.118×10^{-2}	-3.978×10^{-2}	-3.087×10^{-2}	4.013×10^{-2}	2.871×10^{-2}
C_3	2.023×10^{-8}	2.023×10^{-8}	2.023×10^{-8}	2.023×10^{-8}	2.023×10^{-8}	2.023×10^{-8}	2.023×10^{-8}	2.023×10^{-8}
D_3	1.133×10^{-8}	1.133×10^{-8}	1.133×10^{-8}	1.133×10^{-8}	1.133×10^{-8}	1.133×10^{-8}	1.133×10^{-8}	1.133×10^{-8}

TABLE 1.c

INTEGRATION CONSTANTS FOR $\beta = 0.773$

A_i cm	87.732	86.462	83.992	81.382	78.842	76.300	89.000	91.542
B_i cm	98.730	97.460	94.920	92.380	89.840	87.300	97.460	97.460
A_1	-8.871×10^{-3}	-9.567×10^{-3}	-8.923×10^{-3}	-7.977×10^{-3}	-7.785×10^{-3}	-7.779×10^{-3}	-8.848×10^{-3}	-8.218×10^{-3}
B_1	8.946×10^{-3}	9.044×10^{-3}	8.104×10^{-3}	7.589×10^{-3}	7.516×10^{-3}	7.517×10^{-3}	8.562×10^{-3}	8.099×10^{-3}
C_1	1.768×10^{-3}	1.268×10^{-3}	3.185×10^{-5}	-5.122×10^{-5}	-2.362×10^{-6}	2.144×10^{-6}	1.023×10^{-3}	7.266×10^{-4}
D_1	1.432×10^{-3}	1.529×10^{-3}	5.893×10^{-4}	7.452×10^{-5}	3.294×10^{-6}	2.397×10^{-6}	1.047×10^{-3}	5.841×10^{-4}
A_2	-7.108×10^{-3}	-8.175×10^{-3}	-5.909×10^{-3}	1.025×10^{-3}	5.819×10^{-3}	5.995×10^{-3}	-7.744×10^{-3}	-7.459×10^{-3}
B_2	1.630×10^{-2}	1.618×10^{-2}	8.551×10^{-3}	0.9729×10^{-4}	-2.345×10^{-3}	-2.416×10^{-3}	1.485×10^{-2}	1.359×10^{-2}
C_2	-4.690×10^{-3}	-4.281×10^{-3}	-1.925×10^{-3}	-2.656×10^{-4}	2.979×10^{-4}	2.947×10^{-4}	-4.469×10^{-3}	-4.691×10^{-3}
D_2	3.658×10^{-4}	3.080×10^{-4}	1.193×10^{-4}	1.617×10^{-5}	-1.220×10^{-5}	-1.136×10^{-4}	3.733×10^{-4}	4.644×10^{-4}
A_3	-0.1417	-0.1607	-4.250×10^{-2}	3.508×10^{-2}	-5.732×10^{-2}	-0.1338	-8.883×10^{-2}	-3.303×10^{-2}
B_3	-4.385×10^{-2}	-0.1202	-0.1900	-7.824×10^{-2}	-1.635×10^{-3}	-9.081×10^{-2}	-5.254×10^{-5}	1.473×10^{-2}
C_3	0.000	0.000	0.000	0.000	0.000	0.000	0.000	0.000
D_3	0.000	0.000	0.000	0.000	0.000	0.000	0.000	0.000

Consider Figs. 17-20, corresponding to $\beta=0.773m^{-1}$. As the gap leaves the rim, the magnitudes of the stress, which are larger for the model with the gap than for the model without the gap, are reduced when the overlap between the gap and the edge effect zone is reduced. When the gap is located outside the edge effect zone the influence of the gap is reduced. Similarly, when the size of the gap is reduced, Fig. 18, the magnitudes of the stresses decrease. The stress distribution for the gap model converges to the distribution for the continuous model when the gap size goes to zero. Similar behavior is shown in the slope error plots, Figs. 19-20. Furthermore, as β is changed (Figs. 9-16), the qualitative behavior described above is again observed.

In Figs. 21 and 22, the stresses and slope errors (for β = 0.392 m^{-1}), have been plotted in a different manner. In Fig. 21, values of the stress in the adhesive at the gap boundaries are shown for various locations of a gap of fixed size. When the gap is located near the rim (when the vertex end of the gap is between A_0 and A_2) the adhesive between the gap and the rim is entirely in compression. This is a desirable situation - it implies that although the slope errors are higher, the stresses are not tensile, thus minimizing the likelihood that the reflective surface and the substructure will delaminate. As the gap moves away from the rim the adhesive stresses in the region between the gap and the rim change from compressive to tensile. If they were to exceed the strength of the adhesive, separation of the reflective surface from the substructure could occur and, since there is no bonding in the gap region, this separation would extend to point A. When the adhesive between the gap and the rim is in compression, the adhesive on the vertex side of the gap is in tension. These tensile stresses may also exceed the adhesive strength. However, delamination is not as likely to occur because the reflective surface near the rim remains in compression. If delamination should occur to the vertex side of the gap it would be less significant. In Fig. 22, however, a tradeoff appears.

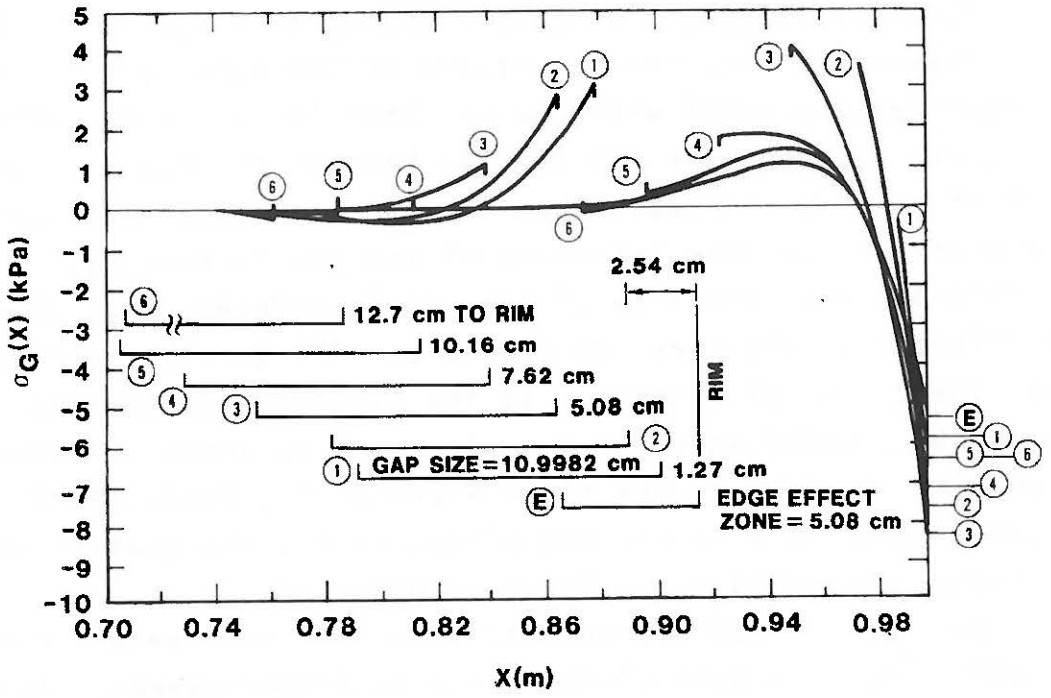

Figure 9. Adhesive Stresses for Various Gap Locations with Constant Size ($\beta = 0.773 m^{-1}$).

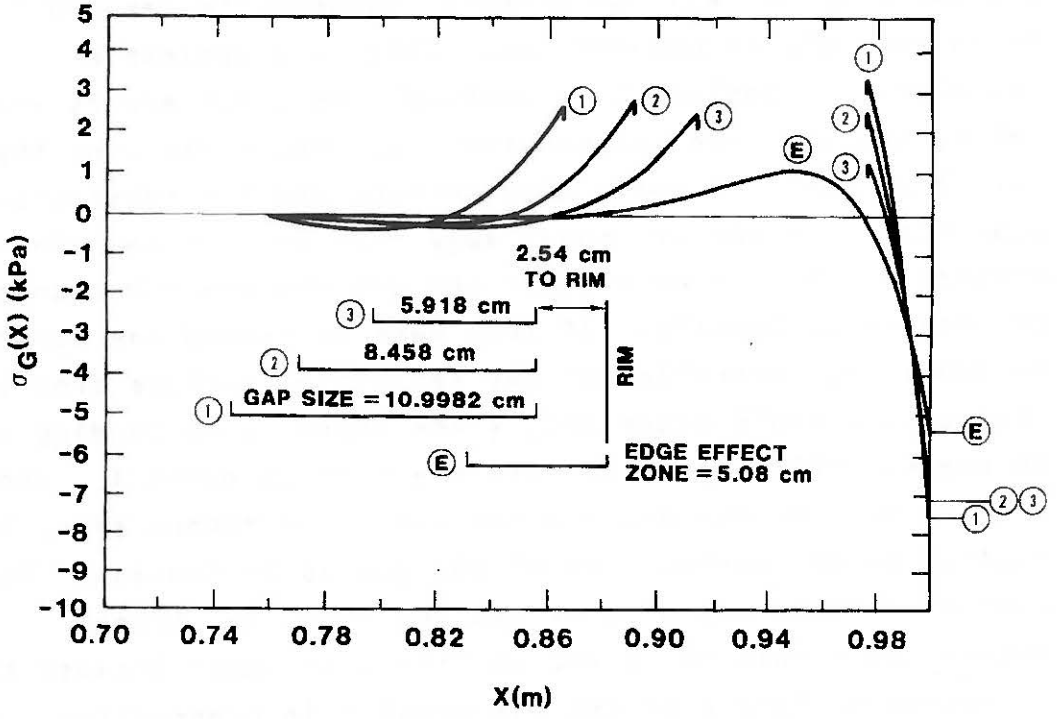

Figure 10. Adhesive Stresses for Constant Gap Location with Various Sizes ($\beta = 0.773 m^{-1}$)

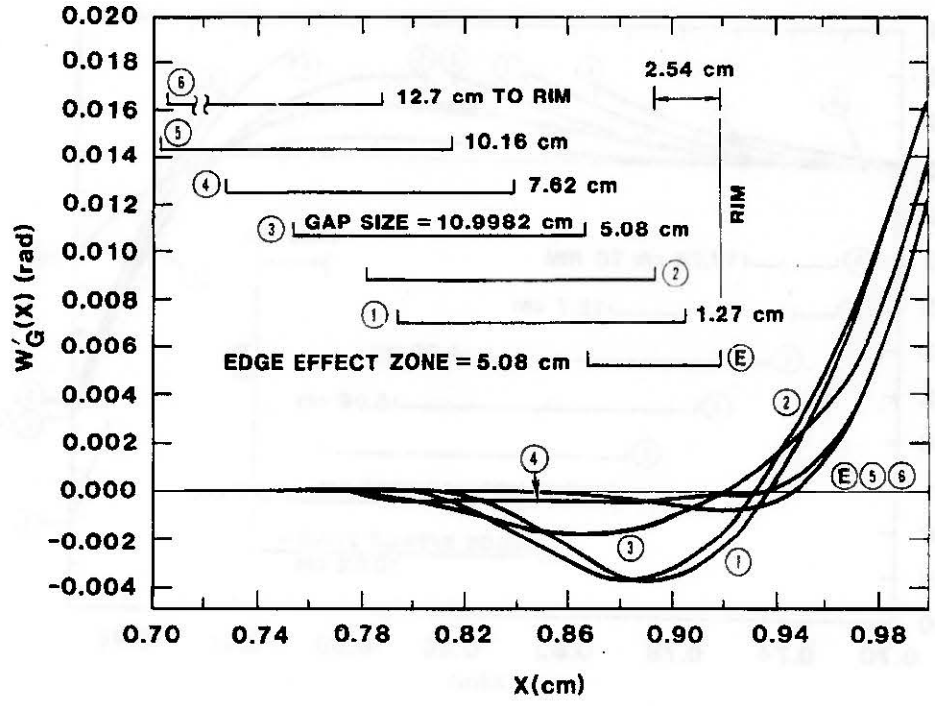

Figure 11. Slope Errors for Various Gap Locations with Constant Size ($\beta = 0.773 m^{-1}$).

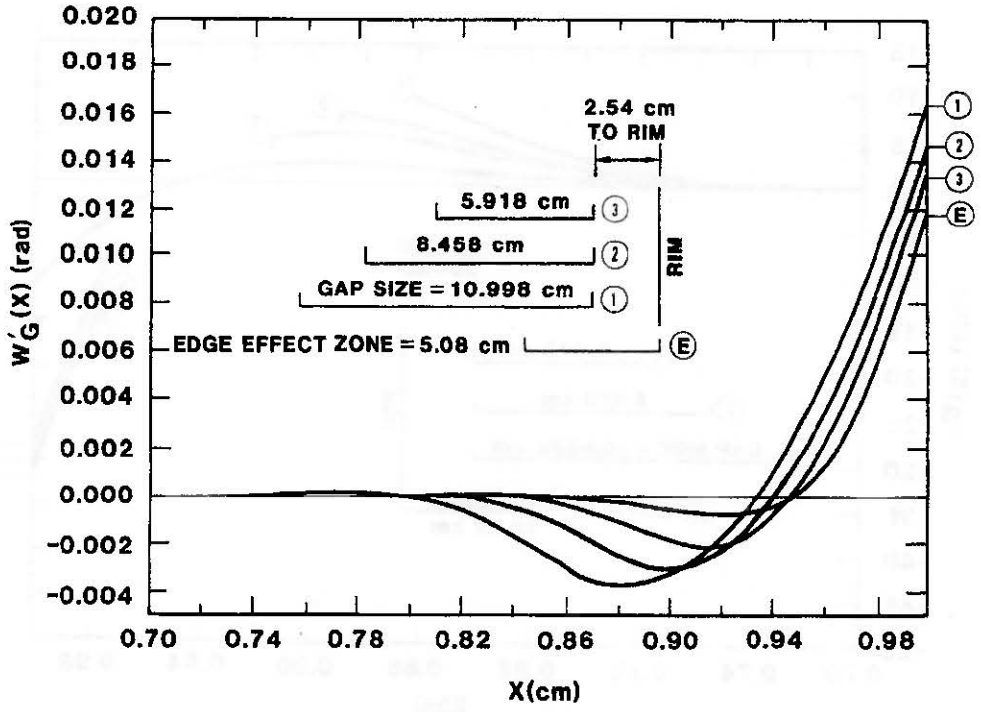

Figure 12. Slope Errors for Constant Gap Location with Various Sizes ($\beta = 0.773 m^{-1}$)

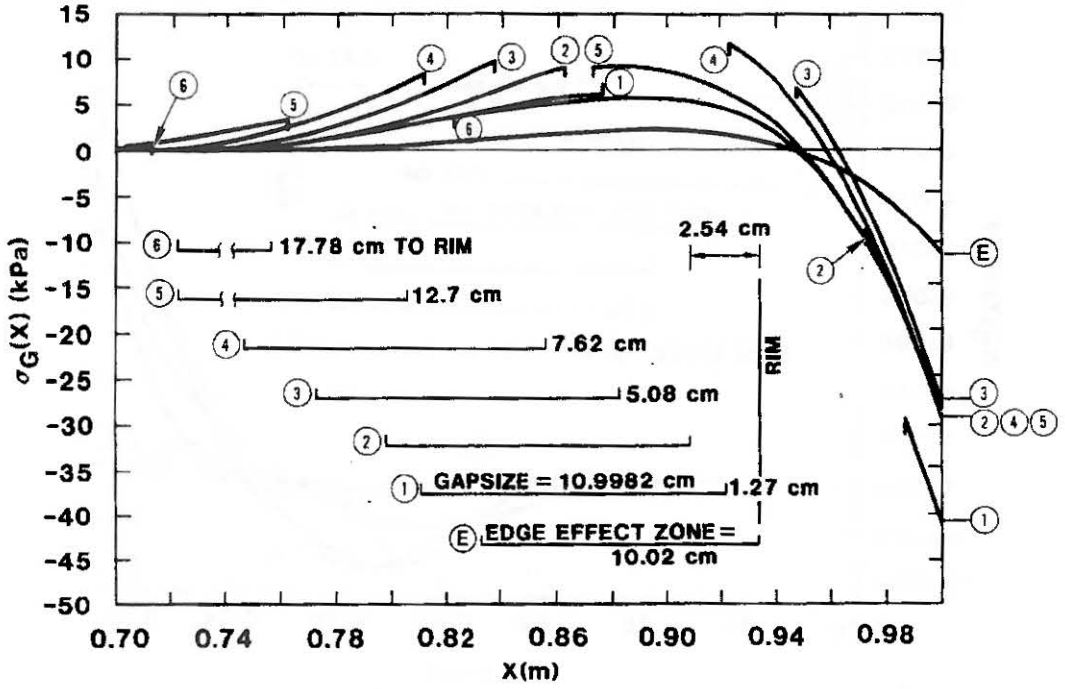

Figure 13. Adhesive Stresses for Various Gap Locations with Constant Size ($\beta = 0.392 m^{-1}$).

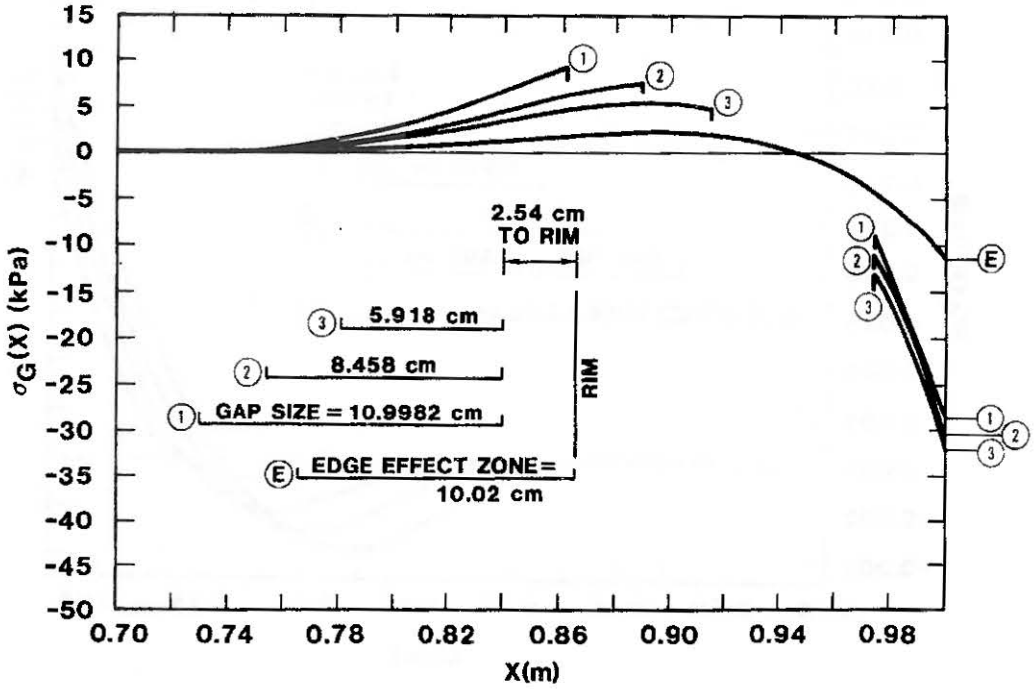

Figure 14. Adhesive Stresses for Constant Gap Location with Various Sizes ($\beta = 0.392 m^{-1}$).

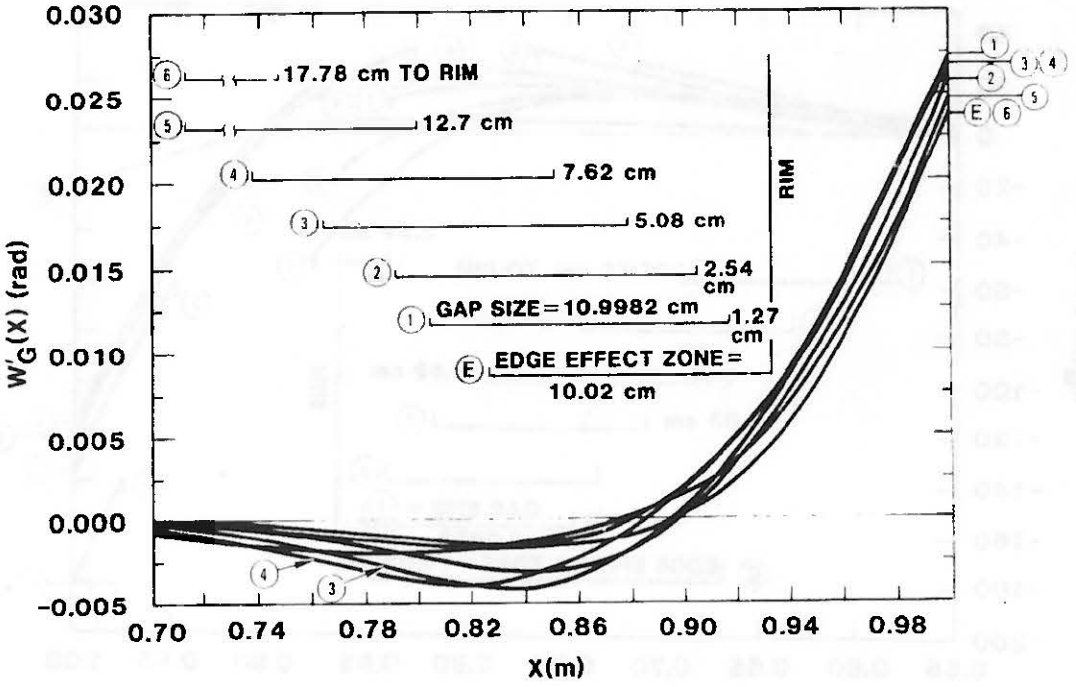

Figure 15. Slope Errors for Various Gap Locations with Constant Size ($\beta = 0.392 m^{-1}$).

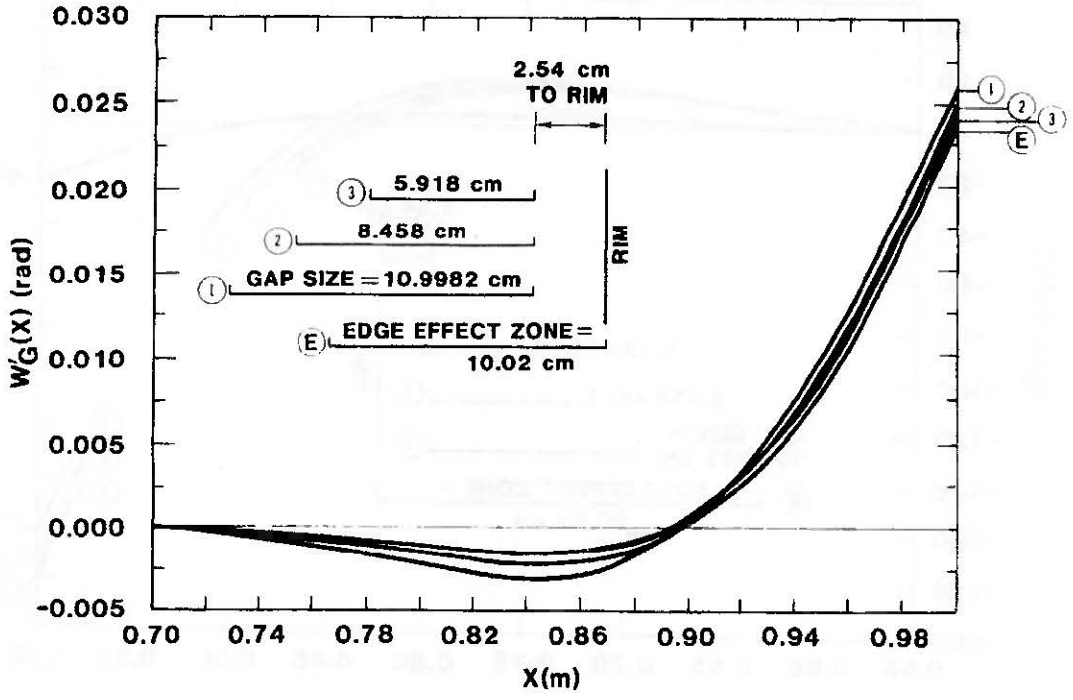

Figure 16. Slope Errors for Constant Gap Location with Various Sizes ($\beta = 0.392 m^{-1}$).

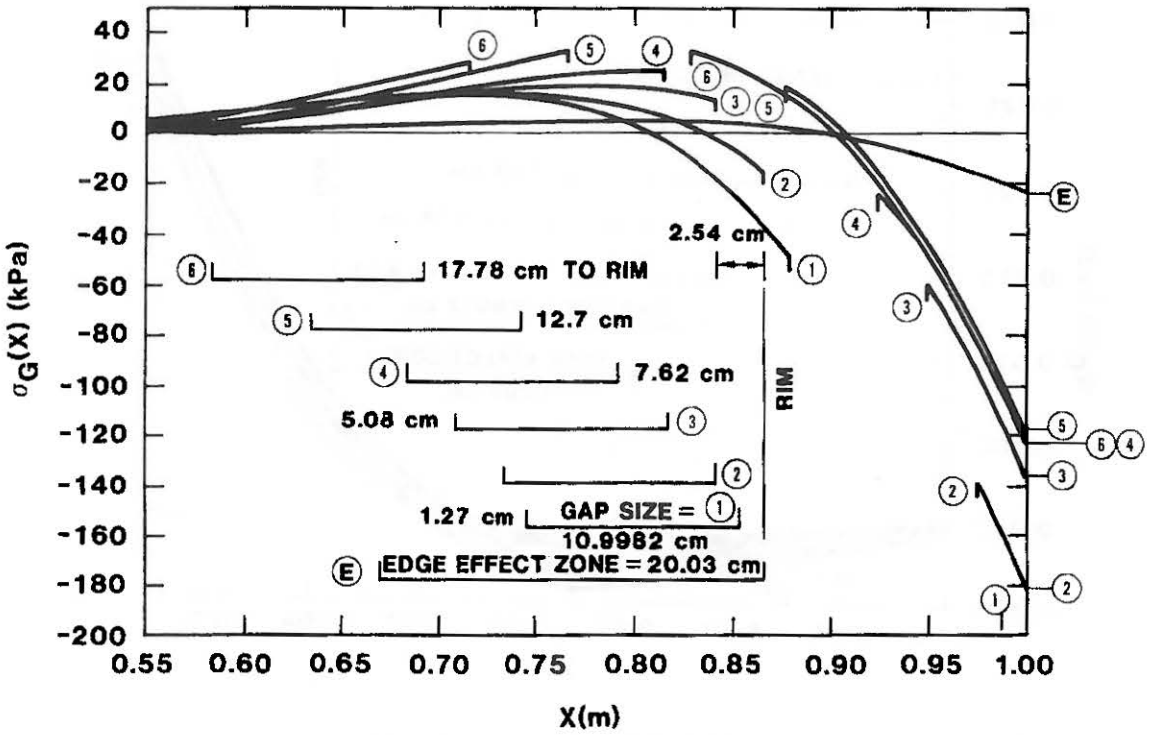

Figure 17. Adhesive Stresses for Various Gap Locations with Constant Size ($\beta = 0.196 m^{-1}$).

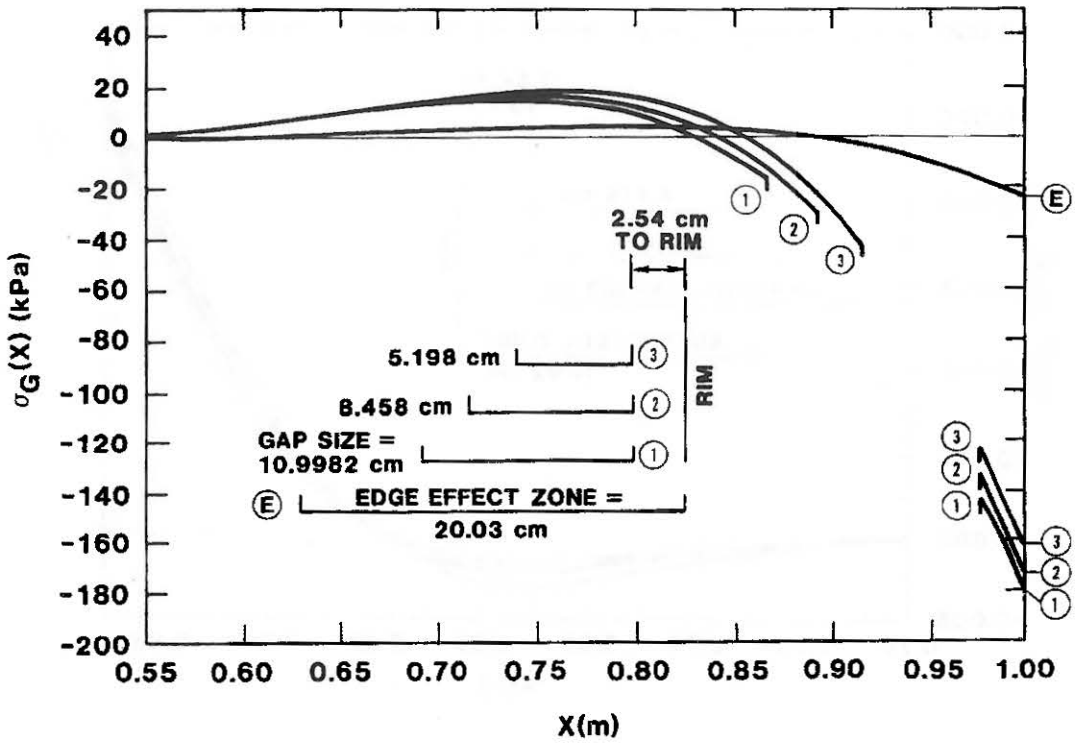

Figure 18. Adhesive Stresses for Constant Gap Location with Various Sizes ($\beta = 0.196 m^{-1}$).

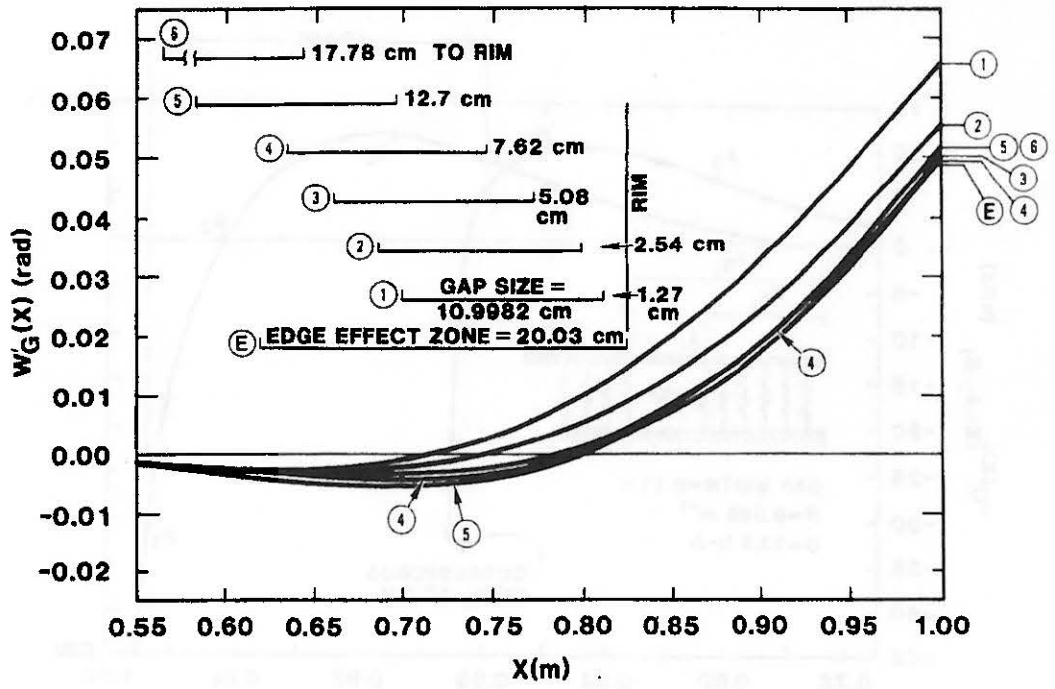

Figure 19. Slope Errors for Various Gap Locations with Constant Size ($\beta = 0.196 m^{-1}$).

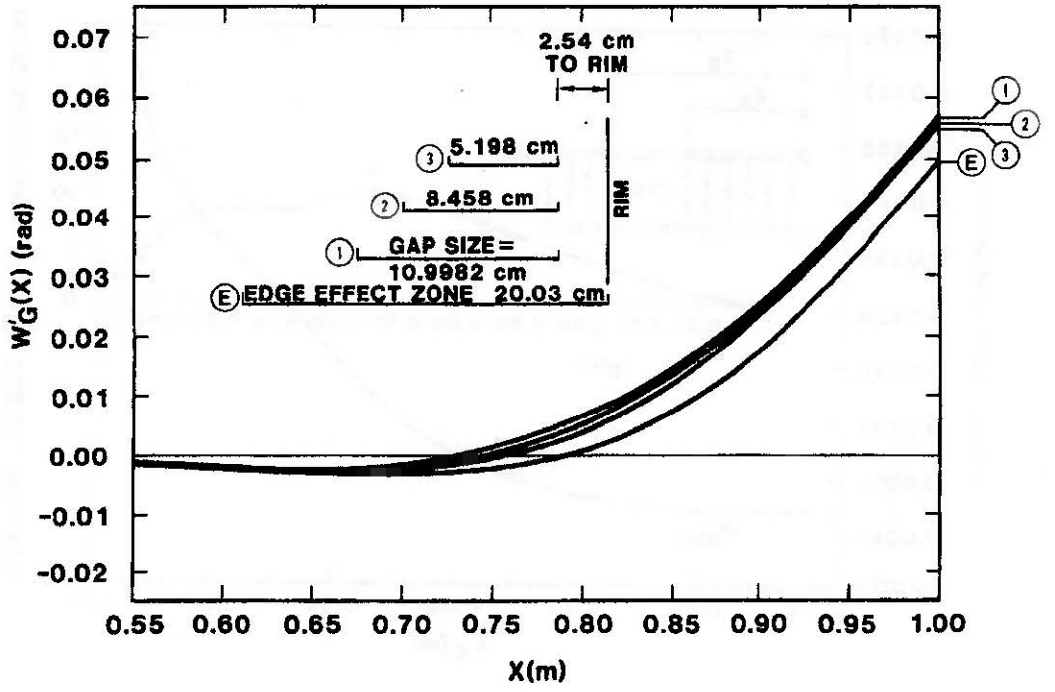

Figure 20. Slope Errors for Constant Gap Location with Various Sizes ($\beta = 0.196 m^{-1}$).

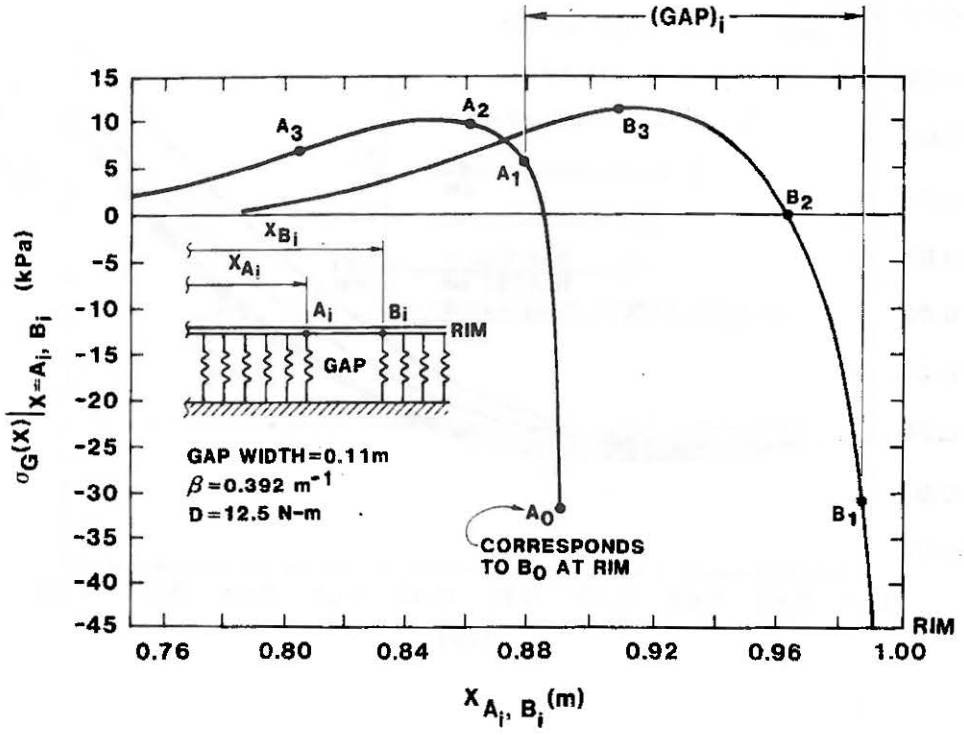

Figure 21. Adhesive Stresses at Ends of Gap (β = 0.392m^{-1}).

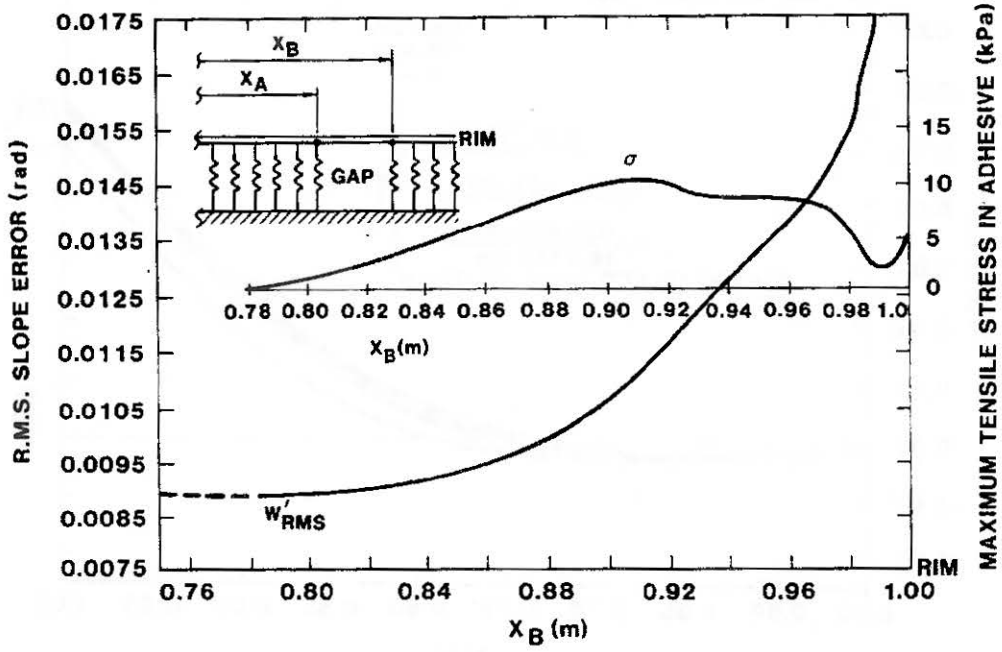

Figure 22. Root Mean Square Slope Error and Corresponding Maximum Tensile Adhesive Stresses (β = 0.392m^{-1}).

When the gap is located near the rim, the adhesive between the gap and the rim is in compression and, as the figure shows, the maximum tensile stress anywhere in the adhesive is low, but the rms value of the slope error* is at a maximum. As the gap moves away from the rim, the value of the maximum tensile stress increases while the rms slope error decreases. Since the increase in maximum tensile stress is minor in comparison to the significant decrease in rms slope error, it appears that moving the gap away from the rim, at the expense of increasing the stresses is more desirable, particularly if the maximum tensile stress is below the failure stress of the adhesive.**

SUMMARY

In this report we have sought to investigate the role of adhesive gaps in bonded panels; in particular, to determine the way they influence the stresses and slope errors that result from edge effects. The influence is significant and some definite conclusions have emerged from this study:

(i) The location of the gap is very influential. As the overlap between the gap and the edge effect zone is reduced, the magnitudes of the adhesive stresses and slope errors are reduced. For gaps very close to the rim, however, the situation is much more complicated and generalizations are difficult to make.

---

* The rms slope error was computed according to the relationship

$$w'_{rms} = \left(\frac{1}{N} \sum_{j=1}^{N} [w'_j]^2 \right)^{1/2} ,$$

where w'_j is the slope error at a point x_j, all points being equally spaced.

** It is obvious that by moving the gap far away from the rim reduces both the maximum tensile stress and the rms slope error to minimum values, however, this particular location contradicts the reasoning behind the existence of the gap, which occurs as a result of a strengthening rib placed in the vicinity of the rim to increase the longitudinal rigidity of the structure.

(ii) The size of the gap is influential; however, only in the sense that as the size decreases to zero, the behavior approaches that which corresponds to the edge effect analysis of a panel with continuous bonding.

(iii) There is a tradeoff between stress and slope error. As the gap is placed farther from the rim, slope errors decrease while maximum tensile stresses in the adhesive on the vertex side of the gap increase. The reduction in slope errors is proportionately greater than the increase in stress, which still remains below the failure level of most adhesives in use. Additionally, as the gap is located farther from the rim, the stress distribution in the gap-to-rim region is no longer purely compressive. A reduction in compressive stresses near the rim is accompanied by the development of a tensile zone near the gap. Cases for which the entire gap-to-rim region is acted upon by compressive stresses are viewed as less susceptible to delamination than those for which a tensile zone is present. Therefore, motivation to place the gap farther from the rim to reduce slope errors is eventually offset by development of tensile stresses near the gap in the gap-to-rim region.

Finally it should be emphasized that these results were obtained for selected values of the material constants and geometry. In practice, one should repeat this analysis to determine which location and size of gap is most desirable.

REFERENCES

1. Reuter, R. C., Jr., and Wilson, R. K., "Contact Stresses on a Thin Plate after Large Displacements to a Full Parabolic Surface", Sandia National Laboratories, Report No. SAND81-2083 (1981)

2. Wilson, R. K., and Reuter, R. C., Jr., "Contact Stresses on a Thin Plate after Large Displacements to a Half Parabolic Surface", Sandia National Laboratories, Report No. SAND81-2563 (1982)

3. Lewis, B. A., "Experimental and Analytical Results for the Structural Behavior of the Sheet Metal Parabolic Solar Collector", Sandia National Laboratories, Report No. SAND82-0045 (1982)

4. Boresi, A. P., Sidebottom, O. M., Seely, F. B., and Smith, J. O., "Advanced Mechanics of Materials", 3rd Edition, John Wiley and Sons, Inc., N. Y., NY (1978).

5. Haskell, K. H. and Vandevender, W. H., Brief Instructions for using the Sandia Mathematical Subroutine library (version 8.0), Sandia National Laboratories, Report No. SAND79-2382 (1980).

APPENDIX A: SUMMARY OF FORMING LOADS, RESULTING STRESSES AND SLOPE ERRORS OBTAINED IN EDGE EFFECT ANALYSIS

Referring to Fig. 8, the forming loads have been determined (see [1]) as follows

$$Q_R = \frac{3D}{32f^2} \quad , \tag{A.1}$$

$$M_R = \frac{2D}{8f} \quad , \tag{A.2}$$

$$M_V = \frac{D}{2f} \quad . \tag{A.3}$$

In addition, the associated forming pressure was found [1] to be

$$P_C(x) = -\frac{5D}{16f^3[1+(x/2f)^2]^{3/2}}\left\{-\frac{1}{40} + \frac{1}{[1+(x/2f)^2]^2}\left(6 - \frac{7}{1+(x/2f)^2}\right)\right\} .$$

The adhesive stresses associated with this distribution is shown in Fig. 3. Removal of Q_R, M_R, M_V yield stress distributions $\sigma_R(x)$, $\sigma_V(x)$ and a distribution of rotated surface nomals $w_R'(x)$, $w_V'(x)$ that are given by [1,2]

$$\sigma_R(x) = -\frac{\beta^3 D}{16(\beta)^2} e^{-\beta(2f-x)}\left[\left(3+4\sqrt{2}(\beta f)\right)\cos\beta(2f-x) - 4\sqrt{2}(\beta f)\sin\beta(2f-x)\right],$$

$$\sigma_V(x) = \frac{\beta^3 D}{(\beta f)} e^{-\beta x}[\sin\beta x - \cos\beta x],$$

$$w_R'(x) = -\frac{1}{64(\beta f)^2} e^{-\beta f(2f-x)}\left[\left(3+8\sqrt{2}(\beta f)\right)\cos\beta(2f-x) - 3\sin\beta(2f-x)\right],$$

$$w_V'(x) = -\frac{1}{2\beta f} e^{-\beta x}\cos\beta x \quad .$$

These distributions are shown in Figs. 4 and 5.

Reproduced by NTIS

National Technical Information Service
Springfield, VA 22161

This report was printed specifically for your order from nearly 3 million titles available in our collection.

For economy and efficiency, NTIS does not maintain stock of its vast collection of technical reports. Rather, most documents are printed for each order. Documents that are not in electronic format are reproduced from master archival copies and are the best possible reproductions available. If you have any questions concerning this document or any order you have placed with NTIS, please call our Customer Service Department at (703) 605-6050.

About NTIS

NTIS collects scientific, technical, engineering, and business related information — then organizes, maintains, and disseminates that information in a variety of formats — from microfiche to online services. The NTIS collection of nearly 3 million titles includes reports describing research conducted or sponsored by federal agencies and their contractors; statistical and business information; U.S. military publications; multimedia/training products; computer software and electronic databases developed by federal agencies; training tools; and technical reports prepared by research organizations worldwide. Approximately 100,000 *new* titles are added and indexed into the NTIS collection annually.

For more information about NTIS products and services, call NTIS at 1-800-553-NTIS (6847) or (703) 605-6000 and request the free *NTIS Products Catalog,* PR-827LPG, or visit the NTIS Web site **http://www.ntis.gov**.

NTIS
Your indispensable resource for government-sponsored information—U.S. and worldwide